Technology Milestone Whitepaper

Laboratory Demonstration of Multi-Star Wavefront Control in Vacuum

Ruslan Belikov (PI), Dan Sirbu, Eugene Pluzhnik, Thayne Currie
(NASA Ames Research Center)

Eduardo Bendek (Institutional PI), Brian Kern, Camilo Mejia Prada, AJ Riggs, Garreth Ruane, Dan Wilson
(NASA Jet Propulsion Laboratory)

Approvals

Released by

E-SIGNED by Ruslan Belikov
on 2020-08-17 22:23:10 GMT

Ruslan Belikov — Date
Principal Investigator, NASA ARC

Approved by

E-SIGNED by Nicholas Siegler
on 2020-08-18 04:16:43 GMT

Nicholas Siegler — Date
Exoplanet Exploration Program Chief Technologist, NASA JPL

E-SIGNED by Brendan Crill
on 2020-08-17 21:00:07 GMT

Brendan Crill — Date
Exoplanet Exploration Program Deputy Chief Technologist, NASA JPL

E-SIGNED by Doug Hudgins
on 2020-08-18 17:33:57 GMT

Douglas Hudgins — Date
Exoplanet Exploration Program Scientist, NASA-HQ

Contents

1 Objective

The objective of this work is to continue to mature a wavefront control technique called "Multi-Star Wavefront Control" (MSWC) from TRL 4 to (component-level) TRL5. MSWC enables the capability to directly image exoplanets and disks in multi-star systems, including important nearby targets such as Alpha Centauri (αCen), with existing direct imaging mission concepts. It is a wavefront control algorithm that requires little or no modifications to the hardware of existing coronagraphic mission concepts. It is also compatible with starshades as long as a DM is present on the telescope.

The specific objectives of this work are to:

- Perform a high contrast laboratory demonstration of MSWC in vacuum, in monochromatic and broadband light, with at least one simple coronagraph and a monolithic aperture (and, depending on testbed availability, with additional coronagraphs and apertures representative of HabEx, LUVOIR and WFIRST [1]).
- Compare and validate models of MSWC on laboratory data.

These objectives flow down to the milestones described in section 3 and prepare MSWC for full system-level tests for specific missions.

2 Introduction and Background

2.1 Motivation

2.1.1 Mission Concepts benefited by this technology

All internal coronagraph missions to directly image exoplanets involve a starlight suppression instrument whose relevant elements are shown in Figure 1. Great strides have been made to mature internal coronagraphs for single star systems, but multi-star imaging is not yet fully mature. The MSWC method uses the existing wavefront control system shown in blue on Figure 1 to enable direct imaging of exoplanets in multi-star systems. A basic version of MSWC (MSWC-0) requires no new modifications or new requirements on the telescope, and the full version (MSWC-s) requires only the existence of a mild grating in the optical train. MSWC is compatible with both coronagraphs and starshades, as long as a DM is present on the telescope (which is already baselined on hybrid coronagraph-external occulter mission concepts such as HabEx).

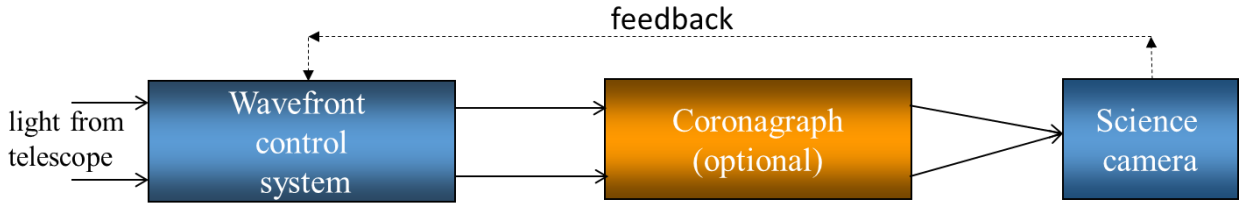

Figure 1. Diagram of a starlight suppression system for a direct imaging mission. Any mission containing the blue boxes can in principle make use of the methods proposed here. (Note: the coronagraph is sometimes upstream of the wavefront control system. For external occulters, a DM must be present on the telescope.)

2.1.2 *Science significance*

The science promised by space-based high contrast imaging missions will result in great leaps in our understanding of warm disks, exoplanetary diversity, dynamics, and atmospheres, a census of exoplanets around nearby stars, and the detection and spectral characterization of Earth-like planets in the habitable zone. However, these missions cannot image multi-star systems with current mature technology, except when the leak and glare of the companion star(s) is negligible or small enough to be removed by post-processing. Therefore, many systems with multiple stars (or optical multiples) are often excluded from the target lists of such missions.

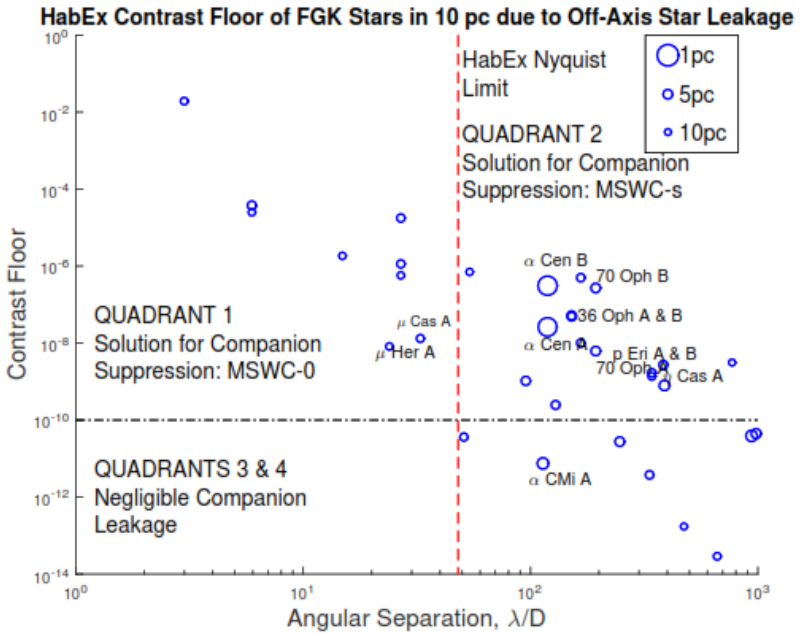

Figure 2. Multi-star systems within 10pc, showing contamination from the companion (using the HabEx mission as an example). The x-axis is the binary separation, at current epoch for a 4 m telescope and λ=650 nm, and the y-axis is the contamination suffered by the on-axis target star from an off-axis companion, due to diffraction and optical aberrations (λ/20 rms end-to-end wavefront error and a $f^{-2.5}$ power spectral density). Values above ~10^{-10} compromise the ability to detect potentially habitable planets.

Enabling the study of multi-star systems is very important because the majority of K-type and earlier stars are in multi-star systems. For example, 5 out of the 7 star systems within 4 parsecs containing K- or earlier type stars are multiple (α Cen, Sirius, Procyon, 61 Cyg, ε Ind), and only two are single (ε Eri, τ Cet).

The potential benefit to science yield can be better estimated by first assessing the fraction of nearby FGK stars with companions, and then the fraction of those companions that leak too much light into primary star's region of interest. A SIMBAD search reveals that there are 69 FGK stars within 10 pc of the Sun, out of which 42 (61%) have at least one companion. If we assume a 4m telescope (size of HabEx A) with λ/20 rms end-to-end wavefront error and a $f^{-2.5}$ power spectral density, then 25 of the stars suffer more than 10^{-10} contrast contamination from the companion and 12 that suffer more than 10^{-7} (see Figure 2). Although the exact amount of contamination depends on many specific details (size of the aperture, type and amount of error, epoch, and location of region of interest), it is clear that MSWC will significantly increase the yield of planets, including Earth-like ones. Furthermore, it will enable new science specific to binary star systems.

2.1.3 *Science highlight: α Centauri*

The αCen system represents a particularly attractive target for direct imaging missions, except for the fact that it is a binary system. Aside from binarity, the A and B stars of the system are unusually favorable low-hanging fruits that are 3 times easier than the next easiest target by almost any metric (see Figure 3, left). In particular, the next closest star earlier than M-type (ε Eri) is 2.4 times as far, and is known to have a thick disk that may interfere with detection of small planets. The next star of comparable proximity to α Cen is Barnard's star, which is 1.4 times farther, with a dimmer visual magnitude of 10, and a habitable zone only 30mas wide (about 30x smaller than αCen). In fact, the αCenA habitable zone spans such a large angle on the sky (~1") that parts of it are outside the *outer* working angle of many large mission concepts. For a given aperture size, the planetary system around αCen would be imaged in at least ~3x higher spatial and spectral resolution (in the photon-noise limited regime) than around any other star, or have at least ~3x SNR for a given spectral resolution. Due to this fact, a mission not designed to directly image potentially habitable planets may nevertheless still be able to do this around Alpha Centauri. For example, the current predicted performance of WFIRST by the CGI team is ~1e-9 contrast (5-sigma) at ~0.4". This would allow the detection of an Earth twin in gibbous phase around Alpha Cen B (a K-dwarf), if WFIRST could image binary stars. For larger telescopes, the greater sensitivity to planets and spectral features around Alpha Centauri could mean the difference between a mission detecting a biomarker or not.

The right side of Figure 3 shows that an Earth twin around α Cen A (or B) will be very obvious on a mission at least as large as Exo-C (1.5m aperture, [2]), if the companion star could be removed and if the exo-zodi level is similar to Solar. An Earth twin can even be theoretically imaged with a 0.25m telescope with a powerful enough coronagraph and wavefront control system [3,4].

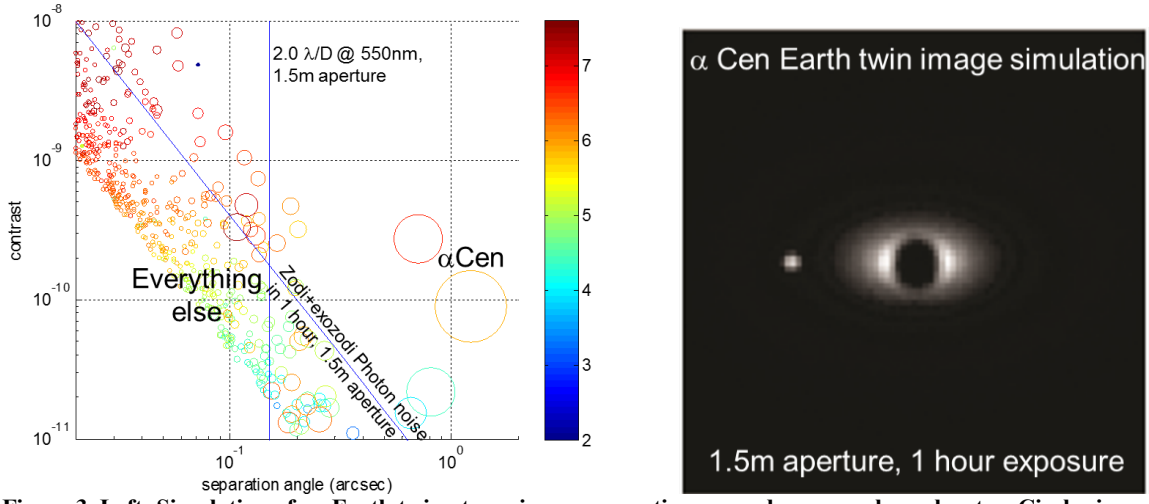

Figure 3. Left: Simulation of an Earth twin at maximum separation around every real nearby star. Circle size and color represent star apparent size and type. For a given aperture, planets around αCen would be imaged with at least ~3x higher spatial and spectral resolution than any other star, if the contamination of the companion star could be suppressed. Right: Simulated image of an Earth twin around α Cen A for a 1.5m aperture (with the PIAA coronagraph). Among included effects were zodi, exozodi = 1 zodi, photon noise.

In short, if α Cen was a single star, it would probably be on the top of the target list for any direct imaging mission, and (if it has potentially habitable planets) would probably end up being the science highlight of any given mission. But, it remains just out of reach, along with many other interesting binaries, because the technology to suppress binary starlight is not yet fully mature.

2.2 Background on MSWC

We briefly summarize the theory behind MSWC, which is covered in more detail in [5, 6]. Let us assume for the moment that a coronagraph or external occulter is completely removing all the light from the on-axis star in a binary system. What remains is then the off-axis star (typically at a super-Nyquist separation), and our job is to suppress the light of the off-axis star that leaks into the region of interest around the on-axis star. Two fundamentally different effects contribute to create this light leak: diffraction and optical aberrations. As a general rule, diffraction dominates close to the star but aberrations dominate far from the star (for typical mirror aberrations). The transition usually occurs on the order of 10 λ/D away from the star. All coronagraphs suppress diffraction, but they do not help with aberrations (except for pinned speckles). A wavefront control (WC) system, or at least some active optical element such as a deformable mirror, is required to suppress optical aberrations. In addition to suppressing aberrations, a deformable mirror is often capable of suppressing diffraction by at least an order of magnitude. Therefore, a second (off-axis) coronagraph is neither sufficient nor necessary to suppress the leak of the off-axis star, while a wavefront control system is both necessary and (usually) sufficient to suppress both the aberrations and diffraction. This goes contrary to the "common wisdom" that the proper way to address the second star in a binary system is to design a coronagraph to block both stars. In effect, the deformable mirror can suffice as a "phase mask coronagraph" for the second star, suppressing diffraction in addition to suppressing aberrations. A separate coronagraph for the second star is only useful if the two stars have an uncommonly close separation (< ~10 λ/D) where light leak caused by diffraction of the off-axis star dominates.

Thus, our solution to binary star suppression (MSWC) is a new wavefront control algorithm rather than a new binary coronagraph design. Wavefront control in binary stars poses two non-trivial challenges as compared to single stars, which we call "sub-Nyquist MSWC" (MSWC-0) and "Super-Nyquist MSWC" (MSWC-s). Sub-Nyquist refers to the case where the region of interest is within the conventional control radius of the DM (for example, 16 λ/D for a 32x32 DM) with respect to both stars. Super-Nyquist refers to regions outside the sub-Nyquist region.

2.2.1 Basic principle of Sub-Nyquist Multi-Star Wavefront Control (MSWC-0)

In general, any region of interest where we wish to detect planets contains a mix of speckles from both stars. The fundamental problem is that these two speckle fields are mutually incoherent. If conventional single-star wavefront control is applied, it will at best remove the speckles of one of the stars but not the other. If single star wavefront control is applied sequentially to suppress speckles from star A, then from star B, that will disrupt the speckle suppression for star A. Thus, in order to suppress both stars, it is necessary to *independently* suppress the speckle fields of each star in the region of interest.

The principle of operation of MSWC-0 is illustrated in Figure 4 with two stars separated by 16 λ/D, in a system (similar to Figure 1) with a DM but no coronagraph. The DM setting has a special MSWC-computed pattern. The dashed red square on the left panel is the (sub-Nyquist) control region of a 32x32 DM with respect to star A. This region can be conceptually separated into 4 vertical sections, controlled by different sets of modes on the DM (with outer sections primarily controlled by modes on the DM corresponding to spatial frequencies with 8-16 cycles per aperture (cpa), and the inner regions controlled by 0-8 cpa). The middle panel of Figure 4 shows the same situation with respect to star B (yellow color).

Finally, the right panel superimposes these two images outlining in white the region where speckles from star A and star B are modulated by two disjoint sets of DM modes: 0-8 cpa for star A and 8-16 cpa for star B. Thus, speckle field of star A can be suppressed by using the 0-8 cpa modes without affecting the star B and likewise the speckle field of star B can be independently suppressed using the 8-16 cpa modes. The MSWC problem is now reduced to two separate conventional WC problems which can be simultaneously solved using a single-star WC algorithm. The same can be done in differently shaped regions, as long as DM modes from star A and star B are "non-redundant" (do not overlap in the region of interest). In general, a 2-star dark zone can be created anywhere within the sub-Nyquist limit of both stars, at the expense of reducing the size of the control region by a factor of two.

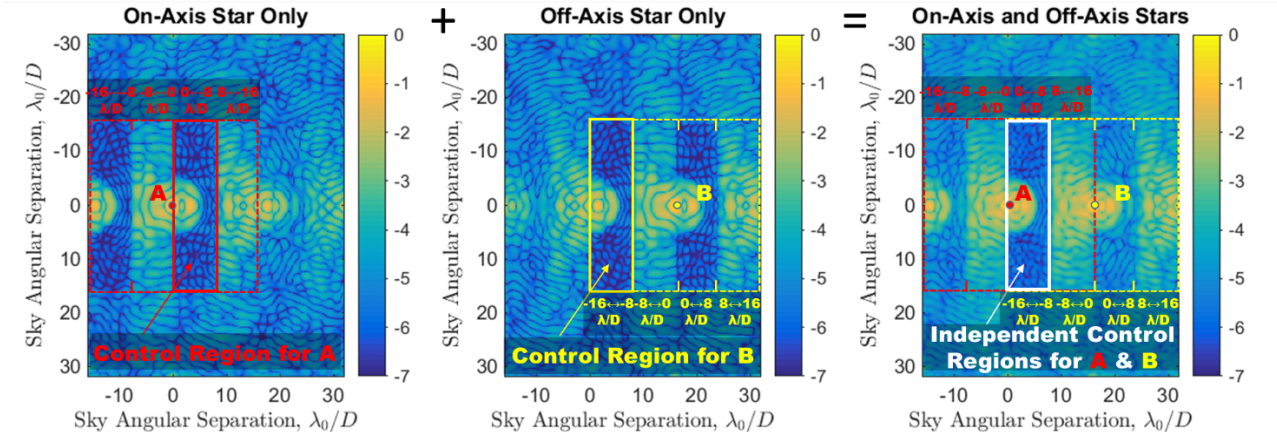

Figure 4. Basic principle behind MSWC: using different modes on one DM to independently modulate light for two different stars. The three panels show a simulation of a focal plane image (for the case of no coronagraph) with two stars and a MSWC-computed deformable mirror setting. Individual stars are shown for clarity (in reality, only the combined image can be obtained on sky). MSWC estimates and corrects both speckle fields independently in the region of interest.

Any mature focal plane-based single-star wavefront control algorithm can be generalized to MSWC-0. These include, for example, classical speckle nulling, stroke minimization [7] and Electric Field Conjugation (EFC, [8]), the latter of which has been used to demonstrate contrast approaching 10^{-10} at JPL's High Contrast Imaging Testbed (HCIT). Most wavefront control algorithms, including EFC, already lend themselves naturally to solving simultaneous wavefront control problems. For example, EFC solves the problem of broadband light suppression by simultaneously solving several narrowband EFC problems (by combining narrowband response matrices into a single larger matrix). In the same exact fashion, EFC and other wavefront control algorithms generalize to MSWC-0 for 2 or more stars, for non-redundant regions of interest.

2.2.2 Overcoming the Nyquist limit

We showed that speckles can be suppressed in the presence of multiple stars as long as the region of interest is non-redundant and within sub-Nyquist separation from all stars. However, if two stars are too widely separated (such as the examples in quadrant 2 in Figure 2, many of which are at 100 λ/D), a region of interest may be at a super-Nyquist distance from one of the stars. To suppress starlight from such systems, we must at least be able to suppress speckles outside the Nyquist limit of the DM (for example, outside 16 λ/D for a 32 x 32 DM). It turns out that this is possible to do if a mild grating is present in the system, which aliases sub-Nyquist DM control modes into the super-Nyquist region [5]. Grating-like structures are already present naturally on

many DMs, such as the 1K and 2K devices made by Boston Micromachines Corporation. This "grating", sometimes called "quilting", is the print-through pattern left over from device manufacture. For some applications that require an absolutely smooth surface, it is undesirable. However, it does enable the creation of dark zones beyond the conventional outer working angle of the DM (for example at 100 λ/D for a 32x32 DM as will be shown in section 1.2.2). Super-Nyquist wavefront control also works in broadband light, although the size of the dark region shrinks [5, 6].

2.2.3 Super-Nyquist Multi-Star Wavefront Control (MSWC-s)

Having the ability to create a single-star dark zone anywhere in the focal plane, including in super-Nyquist regions, allows generalizing MSWC-0 to super-Nyquist multi-star wavefront control (MSWC-s). What is necessary is to ensure that one of the diffraction orders from the off-axis star is within the sub-Nyquist region of the target star. Conceptually, that diffraction order functions similarly to a star at that location, reducing the problem to MSWC-0. For a lattice that has the same period as DM actuators (e.g. DM quilting), there will always be exactly one diffraction order within a sub-Nyquist distance to any point in the focal plane, so a dark zone can in principle be created anywhere. A key requirement, however, is that the energy in the diffraction order needs to be greater than the energy of the speckles in the region of interest, to ensure energy conservation.

Figure 5 shows an illustration of MSWC-s (computer simulation) for the case of stars separated by 70 λ/D. Although the stars are separated by a super-Nyquist distance, diffraction by the DM quilting causes a diffraction order from B to appear within the sub-Nyquist region of A, allowing MSWC-0 to be used with respect to the original star A and the "control diffraction order" of star B.

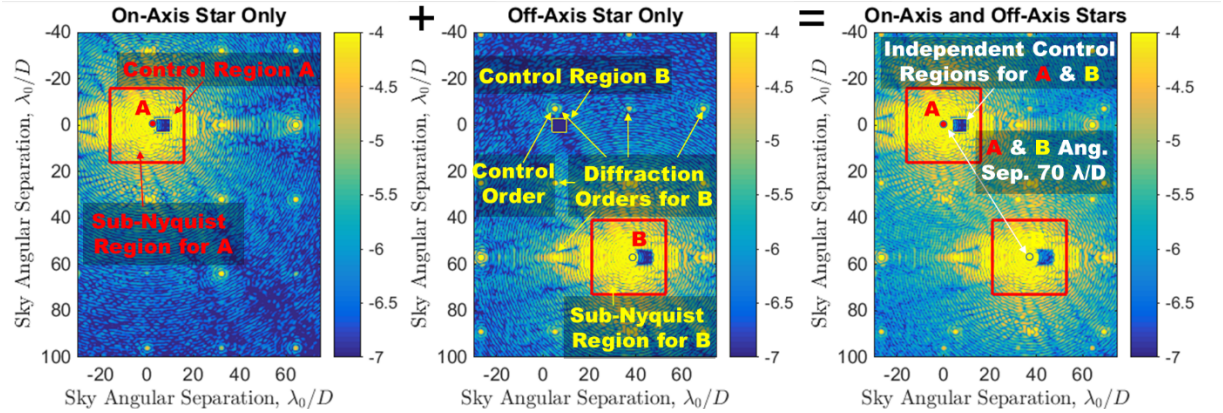

Figure 5. Diagram of super-Nyquist MSWC (MSWC-s). The DM grating diffracts a "control order" of star B into a sub-Nyquist region of star A. Then, MSWC-0 can be applied using the diffracted copy of the star. A shallower dark zone is also created around star B (because the two stars share some common errors).

3 Milestones Definition

Milestone 1 *(end of year 1): Laboratory demonstration, with validated models, of the following performance:*

(1) Raw contrast of 3e-9

(2) In a region between 4 and 8 λ/D

Under the following conditions:

(a) in monochromatic light (within 400-900nm range)

(b) using Alpha Centauri separation and delta-mag; and at least one other representative binary target where the uncorrected contrast floor from the off-axis target starts at 3e-8 or brighter.

Milestone 2 *(end of year 2): Same as milestone 1, except in 10% broadband light.*

Each milestone will be met at a wavelength (or wavelength band) in the 400-900nm range in a static environment, for 3 different stars (α Cen A, α Cen B, and a third star to be selected later). In addition, we plan to benchmark MSWC performance against existing single-star wavefront control methods, to quantify the value added by MSWC. The final results will be documented in formal milestone reports. For a description of "validated models", see deliverable #10 in section 5.7.

4 Experiment Description

The work proposed here represents a continuation of our prior work, which consisted of a completed APRA award (2016-2017) and an ongoing SAT award (2018-2019). As part of that prior work, we have: (a) successfully demonstrated MSWC suppression in computer simulations for several coronagraphs on several missions, including WFIRST, LUVOIR, HabEx, and ACEND (see Figure 6); (b) are in the process testing MSWC with a deployed instrument (SCExAO); (c) successfully demonstrated the basic principles of MSWC in the lab (section 4.3); and (d) are in the process of laboratory testing MSWC with a coronagraph at the NASA Ames Coronagraph Experiment testbed (ACE, see section 4.3).

The work proposed here will continue maturing MSWC by testing it with a coronagraph in *vacuum* as well as in *broadband light*, taking advantage of deeper contrast levels typical of JPL's HCIT. Our general approach is to (conservatively) use the simplest possible coronagraph as a baseline, in order to eliminate all coronagraph-related complications and focus on what we currently perceive as the top risk of MSWC: super-Nyquist suppression of speckles in broadband light. We plan to use a classical Lyot coronagraph with an unobstructed pupil, consisting of a mild diffraction grating to enable Super-Nyquist wavefront control, a hard edge disk occulter (3 λ/D in radius) and an undersized Lyot stop. Although the classical Lyot coronagraph is not optimal in terms of inner working angle and throughput, its simplicity makes it less risky for deep contrasts demonstrations, with < 4e-10 having been reached in a 10% band [9].

Using a simple coronagraph is relevant for other coronagraphs because the top risks of MSWC have to do with suppressing the off-axis star in broadband, which is not expected to be strongly coronagraph dependent. (The off-axis star is not in general blocked by a coronagraph, so its

speckles will be affected only by the pupil and Lyot stops, which are usually high throughput and achromatic.) That said, demonstrations with more advanced coronagraphs are more relevant for TRL5 on missions like LUVOIR and HabEx. As long as more advanced coronagraphs (for example, the Vector Vortex) can reliably achieve ~10^{-9} contrast levels in broadband light in single-star mode, our MSWC tests can be performed with those more advanced coronagraphs instead of the classical Lyot, at no additional cost.

Our work will consist of designing the MSWC mild diffraction grating, and modeling the system (Section 4.1), fabricating the diffraction grating and coronagraph masks (Section 4.2), initial validation at ACE (Section 4.3), testing at HCIT-2 (Section 4.4), as well as analyzing the data and validating the model. This will be combined and iterated according to the plan and schedule shown in section 7.

MSWC is also compatible with other coronagraphs and pupils. If we meet our milestones and reach component-level TRL5 with remaining schedule margin available, we plan to test towards *system*-level TRL 5, including tests with other coronagraphs, pupils, and with injected jitter levels.

4.1 Computer-based simulations and modeling

As part of our precursor work, we have simulated MSWC on many different types of coronagraphs, missions, as well as target separations and delta-mags, using MATLAB diffraction propagation code (which has been validated against PROPER in the past). Based on these simulations, it appears that with a properly designed grating, MSWC can handle a wide variety of stellar separations and delta-mags, with the most challenging cases being stars that have a separation closer than ~10 λ/D, or where the off-axis companion is an order of magnitude or more brighter than the on-axis star. Most binaries of interest to a given mission do not fall into those categories (see, for example, Figure 2), so MSWC should make it possible for a given mission to survey the planetary system of almost any nearby binary star.

The code is based on a MSWC generalization of Electric-Field Conjugation [6]. Some of the mission simulations are shown in Figure 6, showing compatibility of MSWC with a variety of apertures and coronagraphs [10].

We will use this code to design and optimize the mild grating for MSWC-s, as well as maintain a model of the testbed layout in parallel with lab demonstrations. An initial feasibility check of MSWC with the coronagraph we are baselining to test in this proposal is shown in Figure 7. In addition, Figure 8 shows a similar feasibility check for the PIAACMC coronagraph which we are developing as part of another SAT/TDEM program (for single-star imaging), and which synergizes with the work proposed here. Our PIAACMC development program represents a readily available additional architecture for MSWC tests in this proposal, which can be tested with MSWC using any schedule margin that is not used up. In addition, it can serve as a backup architecture.

Following initial checks by computer simulation, we propose to perform trades in order to optimize the design of the mild grating as well as the algorithm parameters to achieve the best performance in terms of size of dark zone, contrast, bandwidth, and stroke of the DM. We will also simulate and verify the actual end-to-end layout, carefully accounting for all important components and potential limiting factors.

As part of our prior work, we have also ported our simulation code to the ARC Hyperwall Cluster computing facility, enabling rapid trades by simulating many MSWC runs in parallel with different parameters. This is not necessary for the success of the proposed work, but represents an opportunity to further optimize the performance of MSWC and enhance the work proposed here.

Finally, we also conducted a trade study of grating requirements. The main conclusions of this study relevant to this work are:

(a) The diffraction orders need to be bright enough such that the energy contained in each diffraction order is much greater (about a factor of 10) than the total energy contained in desired uncorrected dark zone(s) within a sub-Nyquist region of that diffraction order. (Typically, this means that for a dark zone of 10x10 l/D in size, the contrast of the diffraction order needs to be at least 200 brighter than the contrast of the uncorrected speckles.) If this condition is not satisfied, we observe an increase in DM stroke and a degradation of planet Strehl, which gets worse as the diffraction order strength decreases. The brightness of diffraction orders should also not be too bright, because inserting a grating in the system slightly decreases throughput and produces extra speckles.

(b) The grating present on BMC DMs is often sufficient to dig dark zones in most scenarios, but using a standalone grating with a tuned diffraction order strength usually improves DM stroke and Strehl (or alternatively, a dark zone can be made larger).

(c) As long as the grating produces a diffraction order of a desired strength at a desired location, the exact geometry of the grating mask does not appear to be important. (For example, it could consist of a periodic lattice of dots, squares, or a grid of lines, and can be a 1D grating instead of 2D.) This geometry can be tuned to create a desired dependence of diffraction order brightness on its order.

(d) We found that super-Nyquist dark zones are possible even when diffraction orders are not sharp (e.g. when gratings are not perfectly periodic – for example, when quasi-periodic structures on certain shaped pupils inadvertently produce bright speckle regions in the focal plane that look like distorted diffraction orders). Therefore, it appears that the trade space of MSWC gratings extends beyond perfectly periodic gratings, and has a richness that we have only begun to explore. We will continue this exploration, but for purposes of the work in this white paper, simple periodic 2D gratings appear to be sufficient, and first-order requirements are clear.

Running models of the testbed as well as using testbed results to calibrate and validate models is also an important component of laboratory demonstrations and milestones, and a critical tool to diagnose limiting factors. By “model validation”, we generally mean that the model reproduces the effects of dominant sources of noise and artifacts to at least an order of magnitude (see section 5.7, deliverable #10 for more detailed description of the deliverable representing model validation).

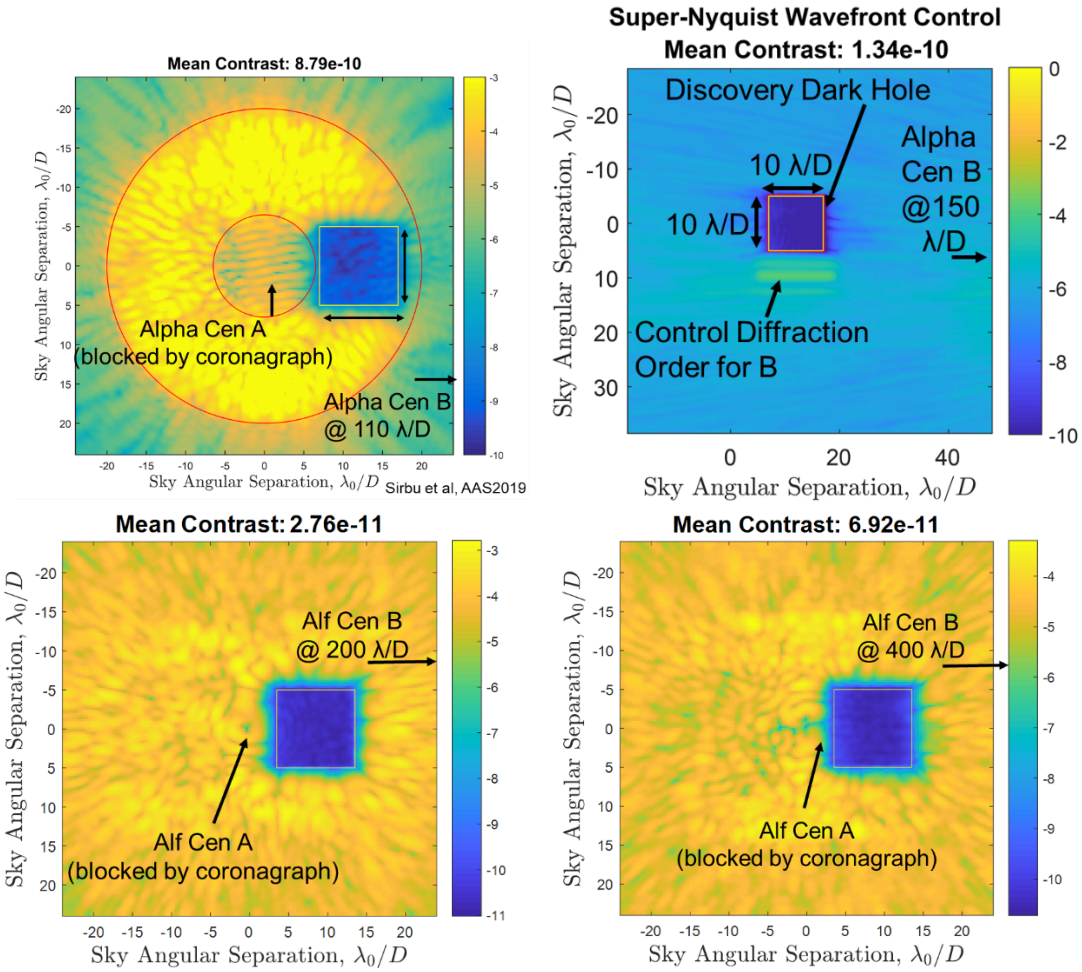

Figure 6. Computer simulations of MSWC on Alpha Centauri A for several different missions and coronagraphs (part of milestone 1 demonstration of the precursor proposal). Top left: WFIRST CGI with the Shaped Pupil Coronagraph; top right: WFIRST with starshade; bottom left: HabEx-A with the charge 6 Vector Vortex coronagraph; bottom right: LUVOIR B with the charge 6 Vector Vortex. All simulations were performed in the presence of static wavefront error, and in 10% broadband light [10].

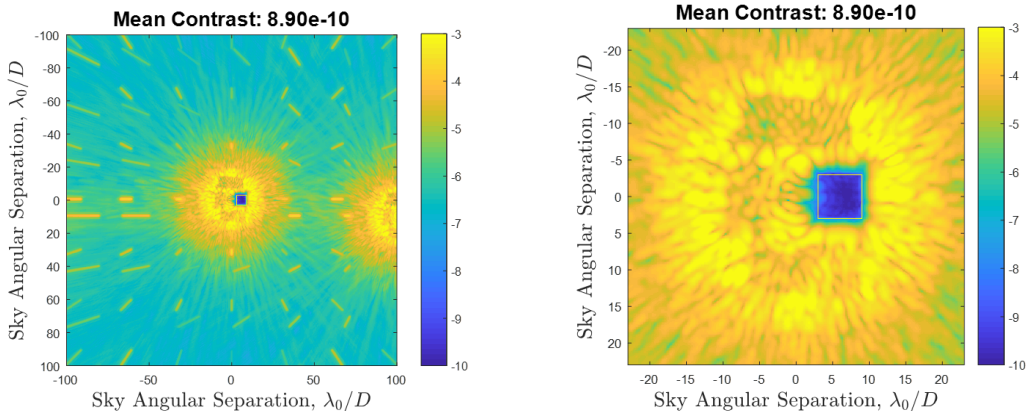

Figure 7. Simulations of MSWC in 10% broadband light using the simple classical Lyot coronagraph, which we propose to test in vacuum as our baseline coronagraph architecture. Left: wide field showing both stars. Right: zoomed in view showing the dark zone.

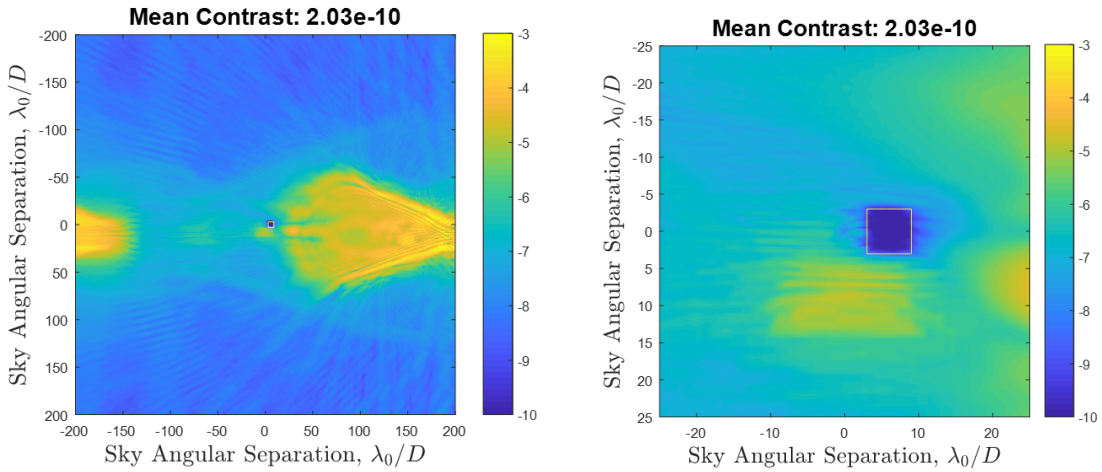

Figure 8. Simulations of MSWC in broadband light using a PIAACMC coronagraph designed for LUVOIR. Left: large field of view; right: zoomed in. This test simulated only the off-axis star (typically the limiting factor), located at 200 λ/D. The PIAA system distorts the off-axis PSF, but nevertheless MSWC-s appears capable of suppressing speckles at super-Nyquist separations (200 λ/D).

4.2 Fabrication of Components

For our baseline tests with the classical Lyot coronagraph, the required components are a flat mirror with a mild grating to enable MSWC-s (examples shown in Figure 9), located in a far field with respect to focus (e.g. conjugate to a pupil plane); a transmissive focal plane mask (opaque disk 3 λ/D in radius); and a Lyot stop. All of these are mature components similar to ones that have been manufactured before and tested with coronagraphs (in the case of the focal plane mask and Lyot stop, below 4e-10 contrast [9]).

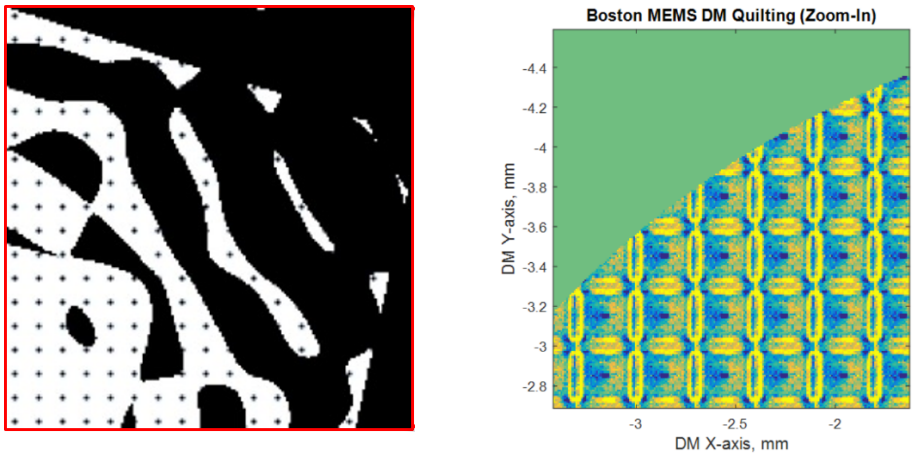

Figure 9. Examples of gratings usable with MSWC. Left: zoom of a standalone amplitude grating integrated with a shaped pupil coronagraph mask (for WFIRST SPC), covering ~1% of the mirror surface. Right: a phase map of a portion of a Boston Micromachines 1K DM, showing a "quilting" pattern left over from the manufacturing process. As long as this pattern can be tolerated in high contrast imaging systems, it enables the super-Nyquist version of MSWC without the need for a standalone grating. However, an optimized standalone grating can improve performance of MSWC-s.

We plan to manufacture the mild grating by imprinting microdots on a flat mirror, using the same process one of our Co-Is (Bendek) successfully used for another SAT / TDEM project [11,12]. The process involves lithographic application of opaque dots on fused silica glass,

performed by University of Arizona. Similarly, the focal plane occulter will be manufactured by the mature process used for existing masks which have been tested at HCIT. The focal plane mask will be nickel on fused silica, and the Lyot stop will be laser cut and anodized aluminum, both made by JPL's Microdevices Laboratory [13]. As a backup, multiple commercial vendors are capable of manufacturing these types of devices.

All masks will be manufactured in batches with bracketed parameters as well as to provide redundancy and use both at the HCIT facility as well as for the initial in-air testing at the ACE testbed.

4.3 Initial validation at the Ames Coronagraph Experiment (ACE)

Initial verifications of the new components will be conducted at the ACE laboratory with MSWC, in order to rule out any major flaws, as well as to validate models of components at mild contrasts before committing to vacuum testing.

The ACE testbed is a state-of-the art facility operating in temperature-stabilized air. It consists of a reconfigurable layout containing a removable PIAA coronagraph, a 32x32 BMC deformable mirror, motorized stages, monochromatic and broadband fiber-fed sources to simulate a star, a data acquisition system, and a file-based interface to communicate with external wavefront control algorithms, compatible with the interface used by HCIT. In addition, it has the ability to simulate a binary star source by moving the fiber source to two different locations, taking two images, and adding them. The resulting sum is equivalent to an incoherent combination of the two images, equivalent to what would happen in the presence of two independent sources, except read noise is increased. For more detail, see [14].

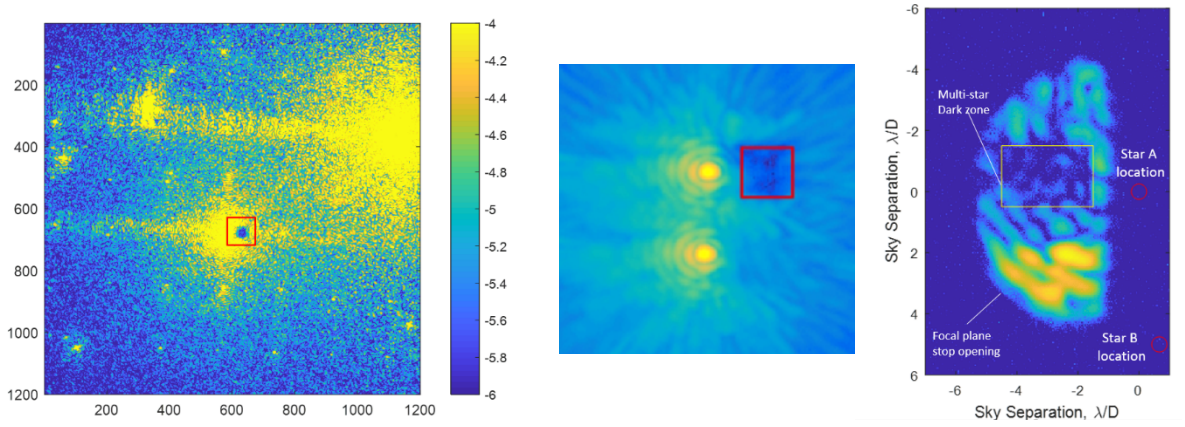

Figure 10. Top: precursor demonstrations of MSWC-s on the ACE testbed, showing basic feasibility of MSWC. Left: MSWC-s in monochromatic light without a coronagraph, showing 1e-6 contrast and at least an order of magnitude suppression of speckles from each star (completed APRA work, [18]). Center: preliminary tests of MSWC-0 in broadband light (completed APRA work, [18]). Right: preliminary laboratory tests of MSWC-0 with the PIAA coronagraph (ongoing precursor SAT-TDEM work).

The ACE testbed is currently being used to develop MSWC in monochromatic light and mild contrast levels, as part of our ongoing SAT-TDEM precursor work. Preliminary demonstrations are shown in Figure 10. This work is scheduled to complete at the end of 2019 and will serve as a starting point for the work proposed here.

4.4 Vacuum testing at JPL's HCIT-2

After initial validation at ACE, we plan to start vacuum testing at the HCIT-2 facility. We are baselining the use of the Decadal Survey Testbed (DST) for this purpose. It is also possible to conduct our program on other HCIT testbeds, adding some degree of flexibility and mitigating schedule risk.

The DST is a general-purpose testbed described in detail in [15], and can be reconfigured between several different types of coronagraphs, including the Vector Vortex, Hybrid Lyot, and Classical Lyot coronagraphs. The input source consists of a SuperK continuum, white light source with a tunable spectral band filter, capable of delivering light with central wavelengths ranging from 400 to 840 nm and with 10 – 100 nm bandwidth (2% - 18% at λ = 550 nm). The white light laser is focused onto an ultrathin precision circular pinhole made by MDL which defines the optical source point. The optical train contains six oversized, off-axis parabolic mirrors (OAPs). A deformable mirror (DM) defines the pupil and redirects light toward a second DM and an OAP2, which produces a focal plane hosting an occulting mask. OAP3 collimates the beam to form a pupil conjugate for hosting a Lyot stop. OAP4 re-focuses the beam to form an image conjugate, which holds a field stop to provide the dynamic range necessary and minimize any stray light, especially from the off-axis star. Finally, OAP5 and OAP6 magnifies and projects the coronagraph image onto the camera. Computer-controlled actuations allow in vacuo swapping of focal-plane masks, Lyot stops, and projection of either the pupil or focal-plane images (via insertion/removal of a lens) onto the camera. The DST is currently configured to use a BMC DM, but may be configured into a Xinetics DM layout (Figure 11). Our experiments are compatible with either type of DMs, but a BMC DM may allow us to test whether the quilting present on the DM obviates the need for a standalone grating. (The amount of quilting on the Xinetics DM is insufficient for MSWC.)

The MSWC tests at the DST will involve two modifications: the insertion of a diffraction grating to extend the DM's controllable region beyond the Nyquist limit, as well as modifying the HCIT software to move the fiber source to two locations to enable a multi-star image, following an identical procedure used in the ACE testbed. See Appendix for more details. The existing motion stage (vacuum compatible Newport LTA) has 0.1μm unidirectional positional repeatability, allowing < 1e-9 contrast to be recovered after moving the fiber source, if using a coronagraph that is not overly sensitive to source displacements, such as the classical Lyot. (For more sensitive coronagraphs, tip/tilt modes on the DM can be used to correct for residual errors in positional repeatability of the fiber source.)

We plan to insert the grating in place of the Lyot stop (labeled as "LS" in Figure 11). As a backup, we identified at least four other locations where the grating can accomplish the same function, shown in blue in Figure 11.

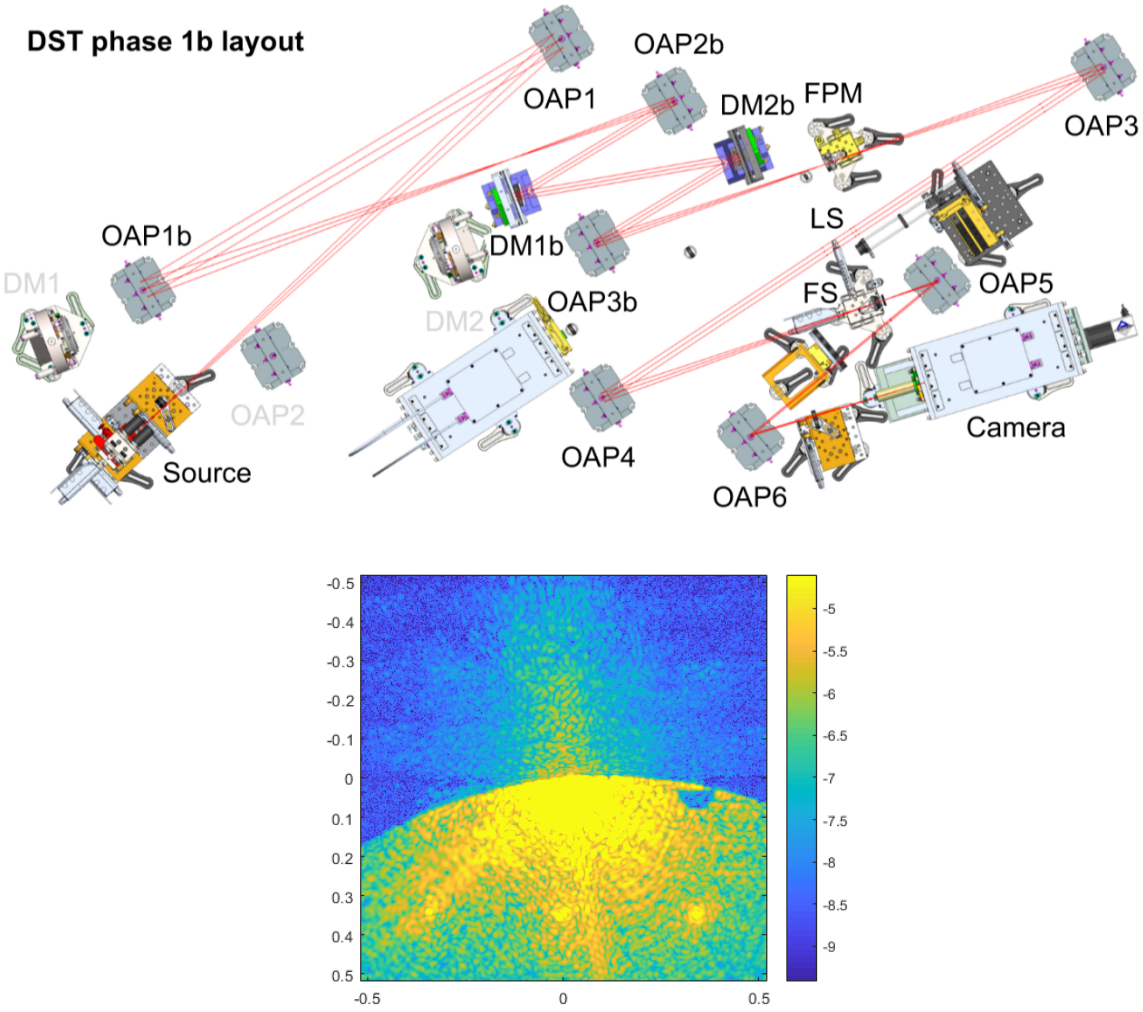

Figure 11. Top: layout of the DST. A diffractive mask is planned to be inserted into the Lyot Stop position, as a baseline (labeled as "LS" in the above figure). However, as long as a DM with sufficient quilting is present in the system, MSWC is possible without an additional grating, albeit with possibly suboptimal performance. Bottom: preliminary demonstration of super-Nyquist wavefront control (a critical component of MSWC-s) on JPL's DST testbed, showing a dark zone at ~50 l/D, 2.6e-8 contrast in monochromatic light.

In addition, as shown in Figure 7, MSWC is expected to be compatible with many different coronagraphs, and using the DST enables easy reconfiguration to those coronagraphs on our program and/or synergizing with other programs on DST. We plan to demonstrate MSWC with the simplest coronagraph (classical Lyot), and test other coronagraphs in case there is schedule margin remaining after the completion of the milestones with the classical Lyot. Other coronagraphs also represent a backup path in case something goes wrong with our baseline path with the classical Lyot coronagraph.

Recently, single star super-Nyquist dark zones were created on the DST in vacuum (by Garreth Ruane), achieving 2.6 x 10^{-8} contrast in monochromatic light at about ~50 λ/D away from the star with a BMC DM. This represents an important first step towards MSWC-s in vacuum for this work.

5 Data Measurement & Analysis

This section describes the details of the data measurements and analysis to reach milestones 1 and 2.

5.1 Definitions

The contrast metric requires a measurement of the intensity of speckles appearing within the dark field, relative to the intensity of the incident star. In the following paragraphs we define the terms involved in this process, spell out the measurement steps, and specify the data products.

The definitions below are based on standard ones established in many previous TDEM projects, but it should be noted that a study by a Science Analysis Group of the ExoPAG [16] proposed new definitions and a figure of merit called the "performance gap", which is based on fundamental concepts in signal detection theory. In order to maintain continuity with past projects, we will continue using the older established definitions for purposes of formalizing milestones and success criteria, but also explore the "performance gap" metric as time permits.

5.1.1 "Raw" Image and "Calibrated" Image

Standard techniques for the acquisition of camera images are used. We define a "raw" image to be the 2D array of pixel values image obtained by reading the charge from each pixel of the camera detector, amplifying and sending it to an analog-to-digital converter. We define a "calibrated" image to be a raw image that has had background bias subtracted and the detector responsivity normalized by dividing by a flat-field image (if the flat field is significantly non-uniform). Saturated images are avoided by choosing appropriate settings for the exposure time, camera gain (if selectable) and source brightness in order to avoid the confusion of camera detector blooming and other potential camera detector nonlinearities. All raw images used for milestone tests are permanently archived and available for later analysis.

5.1.2 DM flat

We define "flat" to be a DM setting in which actuators are set to a predetermined surface figure that is approximately flat (typically, about ~100V for a BMC DM, with appropriate variations to make the surface figure flat).

5.1.3 Star

We define the "star" to be a bare single mode fiber tip, 0.22 numerical aperture with light relayed via the optical fiber from a source outside the optical enclosure wall (e.g. 650 nm frequency-stabilized laser). This "star" is the only source of light in the optical path. It is a stand-in for the star image that would have been formed by a telescope system in a focal plane immediately upstream of the coronagraph. A binary star system is created by moving this fiber to the on-axis and off-axis star locations and then adding the images as described in Sec. 4.

5.1.4 Wavefront control iteration.

We define "wavefront control iteration" to be a measurement of the complex-valued field in the dark zone followed by a MSWC DM correction aimed at removing coherent light in the dark zone

from both stars. Such iterations will be repeated for as many cycles as are needed to reach a desired level of speckle suppression.

5.1.5 Contrast field

The "Contrast field" is a dimensionless map (2D array of numbers) representing for each pixel of the detector, the ratio of its value to the value of the peak of the central on-axis PSF that would be measured in the same conditions (camera setting, exposure time, central source illumination at the input of the instrument) if the coronagraph focal plane mask were removed. Measurement of the contrast field is detailed in sec. 5.4.

5.1.6 Contrast value

"Contrast value" is a dimensionless quantity which is the average value of the contrast field over the dark zone adopted for the experiment. Its measurement is detailed in sec. 5.5. When talking about average value of the contrast field over regions other than the dark zone, we use the term "mean contrast".

5.1.7 "Statistical Confidence"

The measurement of coronagraph instrument contrast at levels better than the success threshold must be statistically significant, ensuring that success is not an artifact of the tails of a noise distribution. This noise, averaged over the dark zone, comprises measurement noise (read noise and shot noise) and systematic noise (photometric calibration).

The measured contrast, averaged over the dark zone, will be considered significantly better than the threshold if it is at least 3σ below the threshold contrast. If the noise were Gaussian, this would correspond to the threshold being outside of a 99.9% one-sided confidence interval about the measured contrast. The σ adopted for this criterion accommodates both the measurement noise averaged over the dark zone and calibration uncertainty. HCIT typically experiences calibration uncertainties on the order of 10% (1-sigma), after the calibration ladder, and it is straightforward to take images with measurement noise well below this level. This means that the measured contrast will have satisfied the statistical confidence requirement if the demonstrated contrast value is ~ 30% better than the contrast threshold stated in the milestone, with the actual numbers depending on more precise noise characterizations which we will do as part of this work.

5.2 Measurement of the Star Brightness

All "contrast" measurements are normalized to the intensity peak obtained when the occulter is removed and the Lyot stop is in place (unocculted star peak brightness). Because the camera dynamic range is typically ~10^4, a so-called "photometric fiducial ladder" calibration procedure is necessary to enable measurements of contrast as low as 10^{-9}. This is done by identifying several fiducial regions in the focal plane, specifically regions a few λ/D wide consisting of speckles whose shape and contrast does not vary much during wavefront control actuation of the DM. In a typical ladder, the first fiducial region is the unocculted PSF itself, the second region can be with the occulter in or out, and having contrast of about 10^{-3}, the third region is with the occulter in, and contrast of about 10^{-6}, etc.

Mean contrast of these fiducial calibration regions is measured iteratively. Specifically, in the zeroth step, the occulter is moved out and the exposure time (and if possible, laser power) is set

such that the unocculted PSF is close to saturation, but still in the linear range of the detector. Thus, contrast of each pixel in the image can be directly computed by normalizing pixel values to the peak brightness of the PSF. Mean contrast in this region 1 (PSF core) is also computed.

Then, during the *n*-th step, assume that the mean contrast of the *n*-th region is known (as with mathematical induction). An image is taken with exposure time (and if possible, laser power) set such that *n*-th and *n+1*-st regions are both seen unsaturated with high SNR on the same image, and within the linear response of the detector. The knowledge of mean contrast in the *n*-th region then allows computing the contrast of each pixel in that image as well as calibrating the mean contrast in the region *n+1*. This completes the induction and allows measurement of contrast down to any level as long as fiducial regions can be found at every step of the induction.

5.3 Measurement of the focal plane scale

The focal plane scale is defined by the displacement (pixels) of the PSF's photocenter in the absence of a focal plane mask in the system for a physical displacement of the light source by fλ/D, where f and D are respectively the focal length and diameter of beam at the input of the system (before PIAA optics). All angular separations given in this document adopt this definition. The PSF photocenter is defined as the intensity-weighted center of the PSF, and is a linear function of the source position at the input of the system. With the above definition, the focal plane scale value obtained is independent of the source offset used in the measurement. We will empirically measure the focal plane scale (both in the lab and in the simulator) by moving the light source by a known amplitude and measuring its photocenter, and verify that the obtained scale matches the value expected from the optical design of the PIAA mirrors and re-imaging optics.

5.4 Measurement of the Coronagraph Contrast Field

Each "coronagraph contrast field" (sec. 5.1.5) is obtained as follows:

1. The occulting mask is placed on the star image.

2. A long-exposure (e.g. seconds) image is taken of the coronagraph field (i.e. the suppressed star plus surrounding speckle field) with the coronagraph focal plane mask in place. A typical geometry of the dark zone is shown in Figure 9.

3. The resulting image is divided by the peak value of the on-axis reference star to produce a "contrast field" image, as discussed in Sec. 5.2.

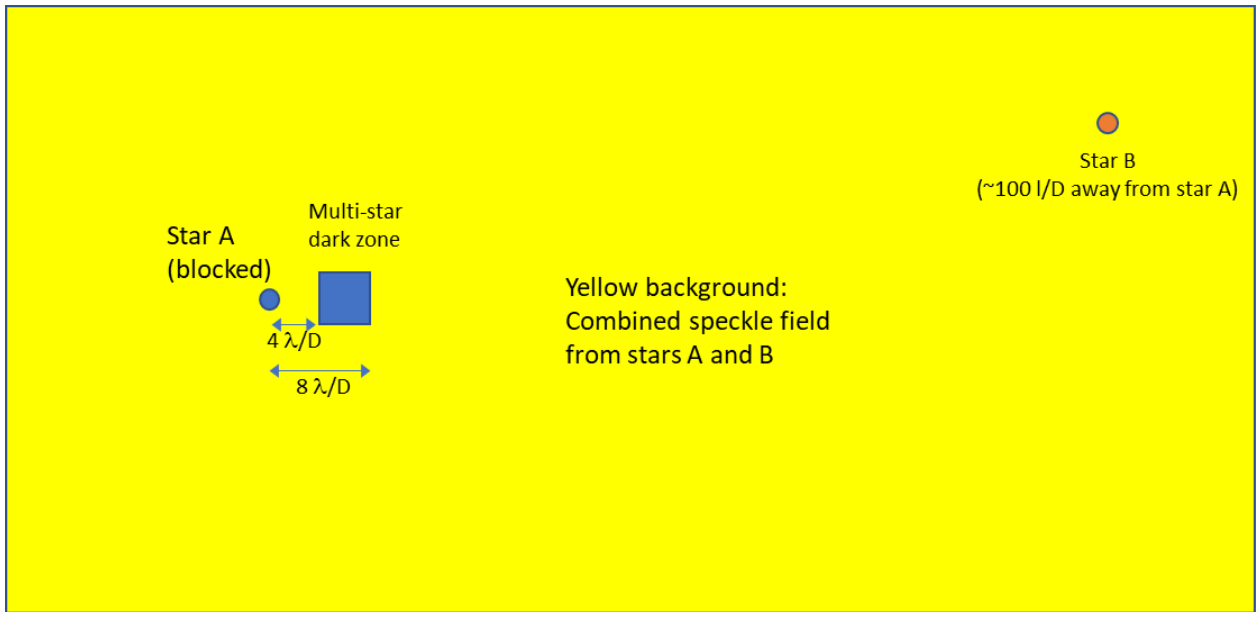

Figure 12. Schematic of the MSWC focal plane, showing the stars and the milestone dark zone. The 4-8 l/D dark zone (4x4 l/D in size) is substantially smaller than what is expected from simulations (at least 10x10 l/D in size, see Figure 6). This smaller dark zone was chosen in order to increase the confidence of achieving the milestone, but we also plan to test larger dark zones once the milestones are completed.

5.5 Contrast value for a single measurement

The contrast field is averaged within the dark zone (Figure 10) to yield the contrast value (Sec. 5.1.6) for a single measurement. This averaging is done over a single image (which itself may consist of a co-addition of consecutive camera frames and separate images of the on-axis and off-axis stars) with no statistical filtering other than removal of detector defects such as bad pixels and cosmic rays.

5.6 Milestone Verification Demonstration Procedure

The Milestone validation demonstration procedure is as follows:

1. The DM is set to flat (Sec. 5.1.2) with a reset of the wavefront control system software.

2. Wavefront control iterations are performed to iteratively converge to settings of the DM actuator driver voltages that give an acceptable high-contrast wavefront solution for the target dark zone. This typically takes several hours, starting from flat, if no prior information is available.

3. When contrast in the dark zone stops improving, a typical high-contrast measurement is made. This measurement is referred to as the contrast field image.

4. All images and data required by the certification data package (Sec. 5.7) are saved and archived.

5.7 Milestone Certification Data Package

The Principal Investigator will assemble a milestone certification data package for review by the Exoplanet Exploration Program and its Technology Advisory Committee. In the event of a consensus determination that the success criteria have been met, the Program will submit the findings of the TAC, together with the certification data package, to NASA HQ for official certification of milestone compliance. In the event of a disagreement between the Program and the TAC, NASA HQ will determine whether to accept the data package and certify compliance or request additional work.

The milestone certification data package will contain the following explanations, charts, and data products.

1. A narrative report, including a discussion of how each element of the milestone was met, an explanation of each image or group of images, appropriate tables and summary charts, and a narrative summary of the overall milestone achievement.

2. A description of the target(s) used (name(s) of the real target(s) we chose to emulate, star separation and delta-mag).

3. Calibrated images of the coronagraph transmittance profile, with graphical cross-sections.

4. Calibrated images of the data set, with appropriate numerical or color-coded or greyscale coded contrast values indicated, and with coordinate scales indicated in units of Airy distance (λ/D), all in demonstration of achieving the milestone elements. Graphical cross-sections of images will also be included.

5. A histogram of the brightness distribution of pixels in the high contrast dark field.

6. A set of contrast measurement values.

7. A description of the residual components of the residual light in the dark zone for each star: static coherent light, dynamic coherent light (due to time-variable pointing errors and wavefront changes too rapid to be fully corrected by the wavefront control loop) and incoherent light (ghosts, polarization leaks).

8. A plot of contrast vs. EFC iteration, as well as a plot showing contrast stability vs. time. This plot will have enough iterations to illustrate the statistical behavior of contrast during EFC operation as well as after it converged.

9. A step-by-step description of all data processing and analysis performed, along with source code and algorithm description. This will be provided in sufficient detail so an independent analysis of the raw data can be applied outside our team.

10. Model validation: plot(s) from computer simulations of testbed, showing contrast as a function of limiting factor(s) strength (for example, contrast vs. jitter). Superimposed on the plot(s) will be

the observed laboratory contrast(s) at the observed level of the limiting factor(s), showing at least an order of magnitude agreement.

6 Success Criterion

Milestones 1 and 2 are to be considered successfully met if the conditions specified by milestone definitions (Sec. 3) are satisfied, with sufficient statistical confidence as described in Sec. 5.1.7. Note that each milestone is to be demonstrated on 3 different stars, in effect requiring 3 separate tests per milestone.

7 Plan and Schedule

7.1 Precursor work

There are two projects led by our team which will serve as inputs to the work proposed here: development of MSWC (which is a formal precursor to this work, see section 4.3) and PIAACMC (which represents a synergy and a backup testbed to DST).

The precursor MSWC project has completed one milestone and has two milestones that are currently in progress: a MSWC demonstration with SCExAO internal source (milestone 2), and a demonstration of 10^{-7} contrast with MSWC at the ACE testbed in air (milestone 3). These milestones are delayed, but we expect to reach both milestones later this year.

For milestone 2, we identified several candidate binary targets to simulate with the SCExAO internal source, and dark zones are currently being created with MSWC at SCExAO. Performance is improving, but has not yet reached 10x in super-Nyquist mode.

Milestone 3 was originally planned to be completed at the ACE testbed, but due to covid-19 and unrelated construction work (building upgrade) impacting our lab, the testbed has not been accessible for many months, and may continue to be inaccessible until November. Therefore, we have identified 2 alternative testbeds that may enable meeting milestone 3 this year: SCExAO, and HCIT (DST). Both directions are currently being pursued. In particular, successful super-Nyquist dark zones have already been created on the DST testbed around the first diffraction order, reaching 2.6×10^{-8} contrast in monochromatic light (see Figure 11, bottom).

The delays of milestone 2 and 3 were primarily due to a combination of: 2019 government shutdown; ACE lab building construction work; team turn-over; and covid-19. Based on this experience, we are planning the following for the work described in this white paper: (a) a more conservative schedule to account for unexpected delays; (b) ability to be flexible and have several backup paths to reaching milestones (for example, multiple backup testbeds and coronagraphs).

7.2 Future work

This effort proposed here spans two years and is diagrammed at a high level in Table 2. It involves 3 design and fabrication iterations, and several iterations of vacuum tests, culminating in milestones 1 and 2 at the end of each performance year, respectively.

The effort will start by performing computer simulations, as well as optimizing the design of the MSWC grating and coronagraph components, and layout, as described in section 4. We will

leverage our existing code as well as supercomputing facilities in order to do trades and a full end-to-end simulation of at least the DST and ACE testbeds with the newly designed components. We will also investigate potential limiting factors in simulation and make sure our system is designed to be robust to them.

The MSWC grating and other components will then be manufactured as described in section 4.2. These types of masks typically take 2 months to manufacture and characterize, including the purchase order process. Multiple sets of masks will be manufactured for redundancy, as well as to provide a set for testing at DST as well as ACE.

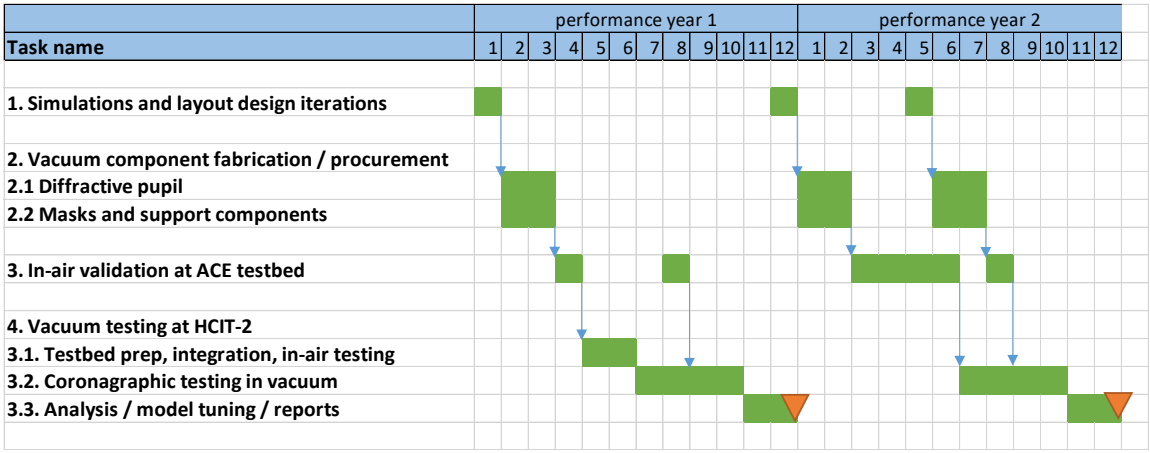

Table 2. Work Schedule diagram. The triangles are milestones 1 and 2 in chronological order. Note: the schedule is notional, pending vacuum tank availability. Performance year start and end are not fully defined and depend on when post-covid-19 lab access can resume, but the intention is to start performance year 1 in the summer of 2020.

In parallel with simulations and mask manufacturing, we will make sure the DST is ready for integration of components and MSWC testing. In particular, we will modify the interface software to enable motion of the fiber source to simulate binary star imaging, and test the communication interface between DST at JPL and the MSWC algorithm at Ames.

Once the MSWC grating and other components are ready, they will be integrated and aligned on the ACE and DST testbeds for initial testing in air, to make sure the system performs as expected, at least down to mild contrasts that are possible in air. Air testing is also important to retire the risk of any major flaws in the design or manufacture of components before starting vacuum tests. Manufacturing several redundant masks also reduces the risk of manufacturing defects.

The first vacuum test is expected to start late 2020 or early 2021, lasting 4 months, followed by 2 months of data analysis. During these tests, we will perform multiple "runs" of MSWC, characterizing its performance, interactively tuning the algorithm and testing the response to different algorithm parameters, analyzing the data for artifacts and limiting factors, and feeding back the results from one run to the next. In parallel with these tests, we will be running computer models and validating them against laboratory data. A detailed description of our test sequence for the first cycle is shown in Appendix A.

Following the completion of the first vacuum test, we will perform an in-depth analysis of the results, paying particular attention to any image artifacts and potential limiting factors. Computer simulations will be used to test whether a potential limiting factor is consistent with observed performance limits, as well as to test ways of mitigating or eliminating such limiting factors, either by algorithm modifications, or minor hardware changes. The ACE testbed will be used during this period to test such changes before the next vacuum test. The result of the two-month analysis

period will be an updated algorithm as well as minor hardware adjustments into the second vacuum test.

Prior to year 2 vacuum tests, there will be a redesign and manufacturing iteration specifically for broadband tests, taking into account all lessons learned from year 1 tests. Year 2 tests will focus on broadband performance, and there will be one final redesign iteration mid-way through year 2, incorporating lessons learned from the first broadband tests.

Experience shows that unforeseen limiting factors often appear in high contrast lab demonstrations. Our strategy of multiple design and testing iterations is tuned to mitigate the risk of such limiting factors and err on the side of caution. Should we succeed in meeting our milestones before the final test cycle, our program allows one or more of the following tests at no additional cost: using the remaining cycles to reconfigure the DST into a different coronagraph and test MSWC with that; test MSWC with our PIAACMC bench at HCIT-2; move towards system TRL 5 tests by testing resilience to tip/tilt modes and jitter. These are not required for the success of our program, but do represent a possible enhancement and synergy with other programs.

8 References and Citations

1] For latest information on HabEx and LUVOIR studies, see: https://www.jpl.nasa.gov/habex/ and https://asd.gsfc.nasa.gov/luvoir/. For latest information on the WFIRST mission, see: https://wfirst.gsfc.nasa.gov/

2] For Exo-C and Exo-S mission concepts, see http://exep.jpl.nasa.gov/stdt/.

3] Belikov, R., Bendek, E. A., Thomas, S., J., Males, J. R., Lozi, J., "How to directly image a habitable planet around Alpha Centauri with a ~30-45cm space telescope," *Proc SPIE* 9605-41, (2015).

4] Bendek, E.A., Belikov, R., Thomas, S.J., Lozi, J., Males, J.R., "Space telescope design to directly image the habitable zone of Alpha Centauri," *Proc SPIE* 9605-40, (2015).

5] Thomas, S., Belikov, R., Bendek, E., "Techniques for High Contrast Imaging in Multi-Star Systems I: Super-Nyquist Wavefront Control," *ApJ 810, Iss 1* (2015).

6] Sirbu, D., Thomas, S., Belikov. R. "Techniques for High Contrast Imaging in Multi-Star Systems II: Multi-Star Wavefront Control," ApJ, 849, *Iss 2* (2017).

7] Pueyo, L., Kay, J., Kasdin, N. J., McElwain, M., Groff, T., Give'on, A., Belikov, R., "Optimal Dark Hole Generation via Two Deformable Mirrors with Stroke Minimization," *Applied Optics,* Vol. 48, pp. 6296, (2009).

8] Give'on A., Belikov R., Shaklan S., and Kasdin J., "Closed loop, DM diversity-based, wavefront correction algorithm for high contrast imaging systems," *Optics Express*, Vol. 15, Iss. 19, pp. 12338-12343, 09/2007.

9] Seo, B.J. et al. "Design description and commissioning performance of a stable coronagraph technology development testbed for direct imaging of Earth-like exoplanets," Proc. SPIE, in prep. (2019).

10] Sirbu, D., Belikov, R., Bendek, E., Henze, C., Pluzhnik, E., "Demonstration of Multi-Star Wavefront Control for Future Missions to Directly Image Exoplanets", 233rd meeting of the AAS (2019).

11] Bendek, E., Guyon, O., Ammons, S. M., Belikov, R., "Laboratory Demonstration of Astrometric Compensation Using a Diffractive Pupil," *PASP 125*, Iss. 932, pp. 1212-1225 (2013).

12] Bendek, E., Belikov, R., Pluzhnik, R., Guyon, O., "Compatibility of a diffractive pupil and coronagraphic imaging," *PASP 125,* Iss. 924 (2013).

13] Balasubramanian, K., et al. "WFIRST-AFTA coronagraph shaped pupil masks: design, fabrication, and characterization", JATIS 2, *Iss. 1* (2015)

14] Belikov, R., et al. "Development of a Method for Exoplanet Imaging in Multi-Star Systems", Technology Development for Explanet Missions White Paper (2017), https://exoplanets.nasa.gov/internal_resources/807_MSWC_WP2017_WP_v6.pdf

15] Ruane, G., Crill, B., Patterson, K., Prada, Camilo M., Seo, Byoung-Joon, Siegler, Nick., "Decadal Survey Testbed Commissioning Roadmap: Demonstrating Technology for Imaging New Worlds," https://exoplanets.nasa.gov/internal_resources/1170/ (2019).

16] Belikov, R., et al. "Direct Imaging of Exoplanets in Nearby Multi-Star Systems", Astro2020 White Paper, http://surveygizmoresponseuploads.s3.amazonaws.com/fileuploads/623127/4458621/249-41b985efb87b071d56e6aaa941af6f33_Astro2020WP_direct_imaging_of_multi_star_systems-v4.pdf

17] Belikov, R., Bendek, E., Pluzhnik, E., Sirbu, D., Thomas, S.J., "High contrast imaging in multi-star systems: technology development and first lab results," Proc SPIE 9904 (2016).

18] Belikov, R., Pluzhnik, E., Bendek, E., Sirbu, D., "High-contrast imaging in multi-star systems: progress in technology development and lab results," Proc. SPIE 10400 (2017).

19] Belikov, R., Bendek, E., Pluzhnik, E., Sirbu, D., S. Thomas, "Laboratory Demonstration of High Contrast Imaging in Multi-Star Systems", AAS Meeting #229, 2017.
20] Belikov, R., Sirbu, D., Bendek, E., Pluzhnik, E., "Methods to Directly Image Exoplanets around Alpha Centauri and Other Multi-Star Systems," AGU Fall Meeting 2017.
21] Bendek, E., Sirbu, D., Belikov, R., Shaklan, S., Riggs, A.J.E., "Enabling super-nyquist wavefront control on WFIRST," Presented at SPIE 10698 (2018).
22] Sirbu, D., Belikov, R., Bendek, E., Henze, C., Riggs, A.J.E., Shaklan, S. B., "Multi-star wavefront control for the wide-field infrared survey telescope," Proc. SPIE 10698 (2018).
23] Sirbu, D., Belikov, R., Bendek, E., Holte, E., Riggs, A.J.E., Shaklan, S. B., "Prospects for exoplanet imaging in multi-star systems with starshades," Proc. SPIE 10400 (2017).
24] Sirbu, D., Pluzhnik, E., Belikov, R., "Modeling of microelectromechanical systems deformable mirror diffraction grating," Proc. SPIE 9904 (2016).

9 List of Acronyms

ACE	Ames Coronagraph Experiment laboratory
APRA	AstroPhysics Research and Analysis
ARC	Ames Research Center
BMC	Boston Micromachines Corporation
CHARIS	Coronagraphic High Angular Resolution Integral Field Spectrograph
cpa	Cycles per Aperture
DM	Deformable Mirror
EFC	Electric Field Conjugation
ELT	Extremely Large Telescope
ESMF	Endlessly single mode fiber
Exo-C	Exoplanet Coronagraph probe mission
ExoPAG	Exoplanet Program Analysis Group
FGK	Stars of type F, G, and K
HabEx	Habitable Exoplanet Imaging Mission
HCIT	High-Contrast Imaging Testbed
HQ	Headquarters
IWA	Inner Working Angle
JPL	Jet Propulsion Laboratory
LUVOIR	Large UltraViolet / Optical / InfraRed Surveyor
MSWC	Multi-Star Wavefront Control
MSWC-0	0^{th} order, or sub-Nyquist, Multi-Star Wavefront Control
MSWC-s	Super-Nyquist Multi-Star Wavefront Control
NASA	National Aeronautics and Space Administration
PIAA	Phase Induced Amplitude Apodization
PSF	Point Spread Function
SCExAO	Subaru Coronagraphic Extreme Adaptive Optics
SIMBAD	Set of Identifications, Measurements, and Bibliography for Astronomical Data
SNR	Signal to Noise Ratio
SNWC	Super-Nyqusit Wavefront Control
STDT	Science and Technology Definition Team
TAC	Technology Assessment Committee
TDEM	Technology Development for Exoplanet Missions
TRL	Technology Readiness Level
WC	Wavefront Control
WFIRST	Wide Field InfraRed Survey Telescope

10 Appendix

10.1 Appendix A: Test plan and procedure for implementing Multi-Star Wavefront Control (MSWC) on DST.

Multi-Star Wavefront Control has several aspects that are best tested and implemented incrementally on DST, ultimately building up to the full MSWC. Below is a recommended sequence of tests as well as a description of what hardware and software modifications are required for each. This sequence is a baseline – depending on the outcome of earlier tests, later tests can be modified or eliminated, or new tests added, as needed.

1. **Single-star super-nyquist WFC (SNWC)**

   This test demonstrates super-nyquist functionality (for a single star), which is arguably the tallest pole of MSWC-s.

   Hardware modifications: None necessary, leveraging the existing DM diffraction orders.

   Software modifications: Standard single-star methods (EFC / Speckle Nulling) should work automatically, except that the code needs to be able to specify and compute super-Nyquist dark zones. Simply choose a dark zone that is super-Nyquist (e.g. 100 l/D) with respect to the on-axis star, and sub-Nyquist with respect to one of the grating diffraction orders. An important consideration is that the code needs to use a FT calculation method that allows specifying computation grids that are not centered around the origin, otherwise the computation is very inefficient. (I.e. straight fft or fftw-based methods work poorly, one needs to use mft or zoomFFT methods.)

   Experiment description and parameters: Start with monochromatic light and very small dark zones (single speckles) and build up to broadband light and large dark zone. Below is an example of a configuration. The dark zone can be placed around either diffraction order, and/or to the north or south of the diffraction order rather than east or west. The important thing is that it is super-Nyquist. 100 l/D is a very useful distance b/c it is the order of magnitude of what's needed for many interesting targets with future missions, such as the Roman telescope imaging Alpha Centauri.

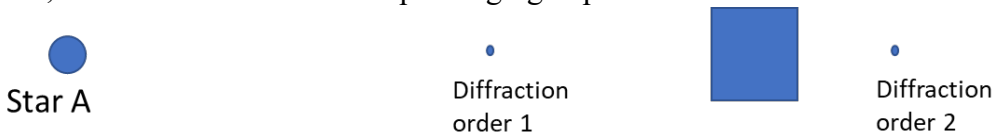

   Success criterion (condition for moving on to the next experiment): 10x suppression of speckles in monochromatic light for a dark zone that is at least 5x5 l/D and ~100 l/D away from the star. Try to do this in 3% broadband as well, but if it does not easily work, log test details and any limiting factor analysis, and move on. We will come back to broadband later.

2. **Double-dark zone single-source test (without fiber motion)**

This test demonstrates the ability of the DM to use low order modes and high order modes to create two different dark zones, without the need to move the fiber. Although it does not demonstrate a multi-star dark zone, it does make sure that the architecture of the code allows specifying and creating two disconnected dark zones that (for the most part) rely on two different sets of modes in the DM. In full MSWC-s, these dark zones would be for two different stars, and overlap in the focal plane.

Hardware modifications: None necessary, leveraging the existing DM diffraction orders.

Software modifications: Standard single-star methods (EFC / Speckle Nulling) should work automatically, except they need to have the ability to specify a dark zone that consists of two disconnected regions, as shown in the diagram below. One is super-Nyquist (e.g. 100 l/D) with respect to the on-axis star, and sub-Nyquist with respect to one of the grating diffraction orders. The other is sub-Nyquist with respect to the on-axis star.

Experiment description and parameters:

Start with monochromatic light and very small dark zones (single speckles) and build up to broadband light and large dark zone. Care should be taken to make sure the two dark zones are non-redundant. (I.e. the set of DM modes that modulate dark zone #1 are completely separate from the modes that modulate dark zone #2. For example, dark zone #1 is modulated by 0-12 cycles per aperture modes, and zone #2 by 13-24cpa. Note that technically speaking, any mode on the DM will modulate both zones to some degree regardless of dark zone shapes and locations, so full non-redundancy is impossible in a strict mathematical sense. However, it is possible to achieve non-redundancy in an approximate sense, where every DM mode modulates at most one zone to first order, which suffices in practice.)

Success criterion (condition for moving on to the next experiment): Simultaneously achieving at least 1e-7 contrast for the near dark zone and 10x suppression of speckles in the far dark zone. Monochromatic light. Dark zones at least 5x5 l/D and the far dark zone is ~100 l/D away from the star.

3a. MSWC-0 DM existence proof.

This test is designed to prove that there is a DM setting which creates a multi-star dark zone in the lab, without (yet) using a realistic way to compute it on sky. A multi-star dark zone is created by alternately turning on star A and star B, and then performing single-star dark zone generation on the same location in the focal plane, as follows.

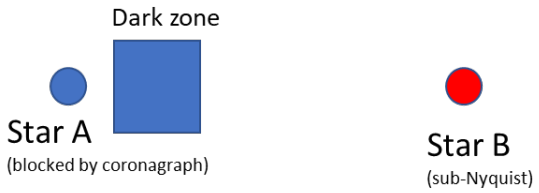

Procedure

1. Select a sub-Nyquist star separation (e.g. 20 l/D) and a non-redundant dark hole (something small to start, e.g. {[4,8], [-2, 2]}, or even smaller)
2. Move the fiber to star location A.
3. Generate dark zone using existing single-star generation code (for N iterations).
4. Move the fiber to star location B.
5. Generate dark zone in the same camera pixel locations, using existing single-star generation code (for N iterations).
6. Repeat steps 2-5 until desired dark zone depth is achieved.

Note: the number of iterations N for each star is (probably) not very important and can be tuned by the operator between 1 and dozens or maybe hundreds, whichever leads to the fastest and best performance. The rule of thumb is that the time spent on steps 2 and 4 should be less than the time spent on steps 3 and 5. N = 10 is probably a good starting point.

Hardware requirements / modifications: Need to be able to move the fiber between star A and B locations (with XX micron accuracy and precision), and have an unvignetted view of both stars A and B.

Software modifications: None necessary if there is a human in the loop moving the fiber. However, automating the entire sequence (2-6) is recommended for this step, probably after trying it manually first.

Success criterion (condition for moving on to the next experiment): Simultaneously achieving at least 1e-7 contrast for the dark zone with star A turned on, and 10x suppression of the speckles with star B turned on. Monochromatic light. Dark zone at least 5x5 l/D

3b. MSWC-s DM existence proof. Same as 3a, but super-nyquist

This test is identical to 3a, except the separation between stars is super-Nyquist (for example, 100 l/D), and all changes that flow from that. In particular, step 3 is changed to single-star *super-Nyquist* wavefront control that was demonstrated by test #1. Be careful to check non-redundancy of the dark zone, because a dark zone used in step 3a may be redundant (unsuitable) for step 3b.

Depending on time pressures and confidence level of the operator, step 3a may be skipped, and we can go straight to step 3b.

4a. MSWC-0 full multi-star correction, but single-star estimation

This test demonstrates the correction portion of MSWC algorithm (not yet the estimation). It also does it in sub-Nyquist mode. In general, the purpose of doing sub-Nyquist tests before super-Nyquist equivalents is to expose and isolate any problems without the added complications of super-Nyquist effects.

Note: depending on time pressures and confidence level of the operator, step 4a may be skipped, and we can go straight to step 4b (super-Nyquist mode). This is especially true if no difficulties were encountered in test 3b.

Procedure

1. Select a sub-Nyquist star separation (e.g. 20 l/D) and a non-redundant dark hole (something small to start, e.g. {[4,8], [-2, 2]}, or even smaller)
2. Generate the EFC G matrix separately for stars A and B using the above dark zone. Note that this dark zone will have different coordinates relative to each star. Then, combine the star A and star B matrixes in to a single one by stacking them on top of each other, in the same exact way that EFC stacks matrixes from different wavelengths, polarizations, or different single point sources when modeling a stellar disk. In other words, the mathematical formalism to handle multiple stars already exists in EFC. (But because it has been developed for a different problem, e.g. broadband, and because the devil is in the details, coding will be required to make sure this formalism is correctly generalized to multi-stars).
3. Move the fiber to star location A.
4. Estimate dark zone due to star A using existing single-star estimation code.
5. Move the fiber to star location B.
6. Estimate dark zone EF due to star B, using existing single-star generation code.
7. Combine estimates from steps 4 and 6 into a single flattened vector in the same exact fashion that EFC combines different wavelength estimates, different polarizations, or different single sources within a stellar disk. Feed this vector through the inverse G matrix to produce a DM correction as usual in EFC.
8. Repeat steps 3-7 until desired dark zone is achieved.

Hardware requirements / modifications: None beyond test 3a.

Software modifications:

The main modification is to EFC algorithm, and is described in step 2 of the procedure above.

However, at this point, it is also recommended to automate the generation of a multi-star image. In the absence of an actual binary star source on the testbed, this can be accomplished as follows: (a) move the fiber to star A position; (b) take an image; (c) move the fiber to star B position; (d) take an image; (e) add the two images together. The image thus produced would have an identical signal and photon shot noise as an image with two real mutually incoherent sources. Instrument noise would be greater (for example, read noise would be sqrt(2) greater) than an image with two real sources, so a test using this method is conservative at least from the point of view of noise. Alternatively, if it is possible to modulate the power of the laser, a multi-star image can be obtained with a single exposure as follows: (a) move the fiber to star A; (b) start a camera exposure; (c) turn off the laser and move it to star B, then turn on the laser; (d) stop the exposure. The signal, photon noise, and read noise in this case would be identical to two real sources, but thermal noise would be greater.

Success criterion (condition for moving on to the next experiment):

Simultaneously achieving at least 1e-7 contrast for the dark zone with star A speckles and

10x suppression of the speckles with star B. Monochromatic light. Dark zone at least 5x5 l/D .

4b. MSWC-s full multi-star correction, but single-star estimation

This test is identical to 4a, except the separation between stars is super-Nyquist (for example, 100 l/D), and all changes that flow from that.

5a. Full MSWC-0

This test demonstrates full MSWC estimation and correction, albeit in sub-Nyquist mode. (For the same reasons as 3a and 4a).

Procedure

1. Select a sub-Nyquist star separation (e.g. 20 l/D) and a non-redundant dark hole (something small to start, e.g. {[4,8], [-2, 2]}, or even smaller)
2. Generate the multi-star EFC G matrix in the same way as in test 4a. In addition, generate the multi-star estimation matrix as well, again following the same mathematical formalism for the two sources in EFC as two different wavelengths or polarizations. During the estimation phase of EFC, independent estimates of speckles for star A and star B will be produced, in exactly the same way as EFC produces different wavelength or polarization estimates.
3. Run full multi-star EFC estimation and correction. Only multi-star images are allowed as inputs to EFC. An example of how to take such images has already been described above, but is also copied here for convenience:
    a. Move the fiber to star location A.
    b. Take image
    c. Move the fiber to star location B.
    d. Take image
    e. Add the two images.

Hardware modifications: None beyond test 3a

Software modifications: The only additional software modification is in EFC estimation, as described in step 2.

Success criterion (condition for moving on the the next experiment): Simultaneously achieving at least 1e-7 contrast for the dark zone with star A speckles and 10x suppression of the speckles with star B. Monochromatic light. Dark zone at least 5x5 l/D.

5b. Full MSWC (i.e. MSWC-s).

This test is identical to 5a, except the separation between stars is super-Nyquist (for example, 100 l/D), and all changes that flow from that.

Depending on time pressures and confidence level of the operator, step 5a may be skipped, and we can go straight to step 5b. This is especially true if no difficulties were encountered in test 4b.

Subsequent tests:

Test 5b completes the demonstration of basic functionality of the full MSWC-s in monochromatic light. Subsequent tests will focus on performance improvements by gradually increasing the band to 3%, the dark zone to 10x10 l/D, and making sure that the test represents a scientifically relevant case (star separation and delta-mag represents a real target, and the dark zone is an interesting region around that target. Current baseline is planets in the habitable zone and out to the stability limit of Alpha Centauri B).

The details of these tests depend on the outcome of tests 1-5, and will be defined once we have more information from tests 1-5.

10.2 Appendix B. Summary of hardware and software changes and requirements:

Hardware:

1. Need to be able to move the fiber between star A and B locations (with 0.25 micron accuracy and precision), and have an unvignetted view of both stars A and B.
2. A mild grating needs to be present in the system. The key requirements of this grating are: (a) the desired dark zone(s) need to fall within a sub-Nyquist distance of at least one diffraction order (this requirement is automatically satisfied for all possible dark zones if the grating periodicity matches the DM actuator periodicity, which is the case for a DM print-through or quilting pattern); (b) each relevant diffraction order (from requirement (a)) needs contain more energy than the total energy of the speckles in the corresponding uncorrected dark zone field. (For our experiments, we expect the peak contrast of the diffraction orders needs to be 2-3 orders of magnitude brighter than the mean contrast of the surrounding speckles, which usually means ~1e-3 or 1e-4 contrast for first order diffraction orders, ~1e-4 or ~1e-5 for second order, and ~1e-5 or ~1e-6 for third order.) If a BMC DM is present in the system, then its quilting may suffice, especially for our initial tests. However, our baseline plan is to insert an optimized grating in the system in the Lyot stop location (other possible locations also exist).

Software:

1. Implementing a multi-star source

In the absence of an actual binary star source on the testbed, we can implement a binary star as follows: (a) move the fiber to star A position; (b) take an image; (c) move the fiber to star B position; (d) take an image; (e) add the two images together. The image thus produced would have an identical signal and photon shot noise as an image with two real mutually incoherent sources. Instrument noise would be greater (for example, read noise would be sqrt(2) greater) than an image with two real sources, so a test using this method is conservative at least from the point of view of noise. Alternatively, if it is possible to modulate the power of the laser, a multi-star image can be obtained with a single exposure as follows: (a) move the fiber to star A; (b) start a camera exposure; (c) turn off the laser and move it to star B, then turn on the laser; (d) stop the exposure. The signal, photon noise, and read noise in this case would be identical to two real sources, but thermal noise would be greater.

Once this functionality is automated, we need a function that takes star separation and delta-mag as inputs, as well as camera-specific parameters (sub-window, exposure time, etc.), and delivers a multi-star image.

2. MSWC algorithm implementation

Generally speaking, there are two ways of implementing MSWC on DST: adding the MSWC feature to JPL-led WC algorithms (e.g. Falco-based), or having ARC-based MSWC code interface DST. Our plan is to start with the former option, but in the end have the capability to do both.

For the latter option (ARC-based), the only thing we require is the interface to HCIT. The ARC team has experience running the old HCIT file-based interface, so in principle it would

suffice to have something like that be available on DST (with the ability to set certain parameters through fits headers such as exposure time, laser power, star separation).

For the former option (JPL-Based, e.g. Falco), the changes are described incrementally in tests above, and also summarized here:

1. The code needs to be able to specify and compute super-Nyquist dark zones (e.g. 100 l/D). An important consideration is that the code needs to use a FT calculation method that allows specifying computation grids that are not centered around the origin, otherwise the computation is very inefficient. (I.e. straight fft or fftw-based methods work poorly, one needs to use mft or zoomFFT methods.)
2. The code needs to have the ability to specify a dark zone that consists of two disconnected regions, with one of them being super-Nyquist (e.g. 100 l/D) in general.
3. Updates to the generation part of EFC. This is done by generating the G-matrix normally but separately for stars A and B, using a given dark zone. Note that a given dark zone will have different coordinates relative to each star. Then, combine the star A and star B matrixes in to a single one by stacking them on top of each other, in the same exact way that EFC stacks matrixes from different wavelengths, polarizations, or different single point sources when modeling a stellar disk. In other words, the mathematical formalism to handle multiple stars already exists in EFC. (But because it has been developed for a different problem, e.g. broadband, and because the devil is in the details, coding will be required to make sure this formalism is correctly generalized to multi-stars).
4. Updates to the estimation part of EFC. The estimation part of EFC again follows the same mathematical formalism for the two sources in EFC as two different wavelengths or polarizations. During the estimation phase of EFC, independent estimates of speckles for star A and star B will be produced, in exactly the same way as EFC produces different wavelength or polarization estimates.